DOI: 10.61782/fa.2023.0367

forum acusticum 2023

CHARACTERIZATION OF ADHESION BY RAYLEIGH MODES GENERATED AND DETECTED BY LASERS

M. Baher[1*] **M. Chrifi Alaoui**[1] **F. Jenot**[1]
M. Ouaftouh[1] **M. Duquennoy**[1]
[1] Univ. Polytechnique Hauts-de-France, Univ. Lille, CNRS, UMR 8520 - IEMN - Institut d'Électronique de Microélectronique et de Nanotechnologie, F-59313 Valenciennes, France.

ABSTRACT

Adhesion is the ability of dissimilar particles to clutch together and is used to describe the contact between two interfaces. It is often considered as the predominant factor for coating reliability in thin-film technologies. Many techniques have been established to estimate the coating-substrate adhesion intensity. In this work, laser-ultrasonics, as a non-destructive non-contact method, is implemented to identify the adhesion level on a structure composed of a polyvinyl chloride film in contact with an aluminum sample. For the generation of elastic waves, a doubled frequency Nd:YAG laser is used. Then, the normal displacement at the surface of the substrate is detected thanks to a heterodyne interferometer of Mach-Zehnder type. Rayleigh modes dispersion curves obtained experimentally are compared to the theoretical ones, which are analytically obtained in order to evaluate the adhesion level as an inverse problem. Moreover, the finite element method is exploited to model the propagation of the surface acoustic waves on the studied sample. Indeed, it is necessary to predict the phenomena that could happen while characterizing a layer on a substrate structure. Finally, this allows to analyze the matching between experimental and numerical results while applying different degrees of adhesion.

Keywords: *Laser Ultrasonics, Adhesion, Dispersion Curves, Non-Destructive Characterization.*

**Corresponding author*: *Mustapha.baher@uphf.fr.*

1. INTRODUCTION

Chemical, mechanical, electrostatic, diffusion and dispersion are mechanisms that describe the phenomenon of adhesion for which the strength is affected by several factors. Evaluating this strength is the primary factor associated with coating quality and the lifetime of the thin film industry [1]. Laser ultrasonics is one of the most efficient non-destructive non-contact testing methods suitable for this purpose. Rayleigh wave is dispersive while propagating in a structure composed of a film on a substrate, due to its interaction with two layers at the same time. Indeed, it is sensitively related to the thickness of the layer and its adhesion to the substrate [2–4].

Diverse studies have been evaluating adhesion strength by means of acoustic waves. Piezoelectric transducers are widely used in research to generate and detect high-frequency elastic waves, which help estimate physical properties such as the adhesion of layers to a substrate. A common issue in studies involving an intermediate adhesive layer at the interface is the difficulty in controlling its thickness [5–7]. Consequently, it is important to have a uniform thickness of the film along the propagation of Rayleigh modes so that the changes in dispersion curves are more accurately caused by the adhesion strength.

The frequency-doubled Nd:YAG can generate surface acoustic waves (SAWs) at the interface between a transparent layer deposit on a substrate, unlike transducers. By generating SAWs at any position at the interface, the impact of adhesion strength on Rayleigh mode dispersion curves can be experimentally determined. Rayleigh wave propagates through the interface and continues on the substrate surface. The normal displacement of the surface is detected at the substrate surface using a heterodyne interferometer.

The transfer matrix method, developed by Thomson and Haskell [8, 9], with the stiffness method by Rokhlin and Wang [10], provides an accurate approach for calculating dispersion curves influenced by adhesion parameters and is presented in the first part. The results of the finite element method are presented in the second part. Finally, the experimental setup is discussed and the results are compared with the theoretical predictions.

2. THEORETICAL BACKGROUND

Three cases of Rayleigh modes dispersion behavior exist, loading case if $c_t'/c_t < 1/\sqrt{2}$, stiffening case if $c_t'/c_t > \sqrt{2}$, and intermediate case if $1/\sqrt{2} < c_t'/c_t < \sqrt{2}$, such that c_t' and c_t are the shear wave velocities of the layer and the substrate respectively [11]. The transfer matrix by Thomson and Haskel is a widely used method in many publications [12–15] for studying adhesion. For a given stiffness K_α, such that $\alpha = n$ and $\alpha = t$ for normal and tangential stiffness respectively, the stresses and displacements are given as:

$$\begin{cases} \sigma_{ij} = \hat{\sigma}_{ij} \\ \sigma_{ij} = K_\alpha(\hat{u}_i - u_i) \end{cases} \tag{1}$$

In this equation, σ and u denote respectively the stress and displacement of the substrate at the boundary, while $\hat{\sigma}$ and $\hat{u}$ correspond to those of the layer.

The theoretical approach considers a homogeneous multilayered structure, for which each layer has density ρ, transversal wave velocity c_t, and longitudinal wave velocity c_l. The transfer matrix method of a multilayered structure is a concept that links the stresses and displacements properties of a layer into a matrix mathematical form. The matrix representation for a single layer on a semi-infinite substrate can be written as [8–10]:

$$[\mathbf{M}] = [M_{\text{Substrate}}(0)]^{-1}[A][M_{\text{Film}}(h_{\text{Film}})][M_{\text{Film}}(0)]^{-1} \tag{2}$$

such that:

$$A = \begin{pmatrix} 1 & 0 & \frac{1}{K_t} & 0 \\ 0 & 1 & 0 & \frac{1}{K_n} \\ 0 & 0 & 1 & 0 \\ 0 & 0 & 0 & 1 \end{pmatrix} \tag{3}$$

Here, $[\mathbf{M}]$ denotes the matrix of stresses and displacements for the structure. The matrices $[M_{\text{Substrate}}(0)]^{-1}$ and $[M_{\text{Film}}(h_{\text{Film}})]$ represent the boundaries between the substrate and the film interface, while $[M_{\text{Film}}(0)]^{-1}$ corresponds to the layer-free surface interface. The dispersion relationship can be determined using the matrix elements, labeled as $\mathbf{M}_{ij}$, from the matrix $[\mathbf{M}]$. Here, i represents the row number and j stands for the column number:

$$\frac{\mathbf{M}_{21} - \mathbf{M}_{11}}{\mathbf{M}_{12} - \mathbf{M}_{22}} = \frac{\mathbf{M}_{41} - \mathbf{M}_{31}}{\mathbf{M}_{32} - \mathbf{M}_{42}} \tag{4}$$

Fig. 1, shows the evolution of the dispersion curves of Rayleigh modes for different values of $k_{n,t}$ propagating through the interface of polyvinyl chloride (PVC) layer of longitudinal and transversal wave velocity $c_{l_{PVC}} = 1900\ m/s$, $c_{t_{PVC}} = 760\ m/s$ respectively, density $\rho_{PVC} = 1300\ kg/m^3$, and thickness $h_{PVC} = 213\ \mu m$, on aluminum (Al) substrate of longitudinal and transversal wave velocity $c_{l_{Al}} = 6400\ m/s$, $c_{t_{Al}} = 3140\ m/s$ respectively, and density $\rho_{Al} = 2798\ kg/m^3$, in the loading case.

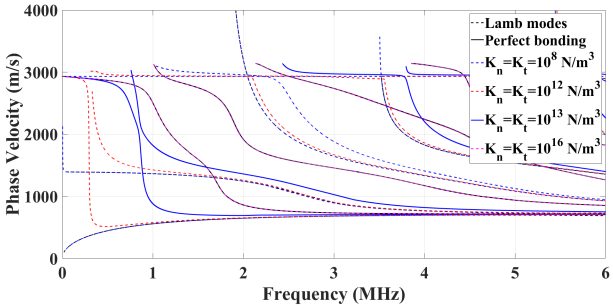

Figure 1. Evolution of Rayleigh modes dispersion curves with respect to different adhesion strength.

When the stiffness is weak, the Rayleigh modes separate and tend towards the Lamb modes of the PVC layer, as well as the Rayleigh wave velocity of the substrate. However, when the stiffness becomes strong, it forms the dispersion curves of Rayleigh modes under perfect contact condition.

3. FINITE ELEMENT MODELING

A Finite Element Modeling (FEM) is performed and the section is split into two parts. The first one covers the essential parameters of aluminum and polyvinyl chloride required for the FEM analysis, along with the model's geometry, meshing, and time step conditions. The results are compared with the theory in the second part.

3.1 Material Parameters and Meshing

3.1.1 Geometry

A squared aluminum block of 9.8 cm length and a thickness of 4.9 cm is used experimentally, along with a PVC film of a measured thickness of $h_{PVC} = 213 \pm 5\ \mu m$ and a width of 2 cm. A two-dimensional geometry in the plane strain structural mechanics model is sufficient for accurate results. To reduce simulation time, the geometry of this 2D model, as depicted in Fig. 2, is summarized as follows:

- Polyvinyl chloride (subdomain D_1): $L_{PVC} = 15.1\ mm$, $h_{PVC} = 213\ \mu m$,
- Intermediate layer (subdomain D_2): $L_0 = 15.1\ mm$, $h_0 = 0.1\ \mu m$,
- Aluminum (subdomain D_3): $L_{Al} = 17.1\ mm$, $h_{Al} = 0.5\ mm$,
- Perfectly Matched Layer (subdomain D_4).
- Source: two points separated by 200 μm.

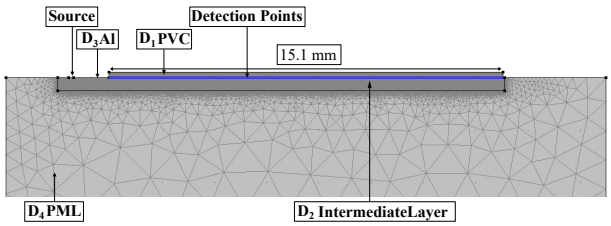

Figure 2. Diagram showing the meshing of the geometry and its dimensions, as well as the detection and generation points.

The interfacial layer represents the adhesion strength, and the thickness is fixed at $h_0 = 0.1\ \mu m$ (negligible thickness less than 0.1% of h_{PVC}), $\nu_0 = 0$, and a density of $\rho_0 = 130\ kg.m^{-3}$ that is 10% of ρ_{PVC}. Finally, the Young's modulus of this layer E_0 links the adhesion parameters K_n and K_t in Eqn. (5) as the following [10]:

$$\begin{cases} K_n = \frac{1}{h_0}\frac{E_0(1-\nu_0)}{(1+\nu_0)(1-2\nu_0)} = \frac{E_0}{h_0} \\ K_t = \frac{1}{h_0}\frac{E_0}{2(1+\nu_0)} = \frac{E_0}{2h_0} \end{cases} \tag{5}$$

3.1.2 Parameters

To apply the parameters to this model, we need to calculate Young's modulus and Poisson's ratio for each material. These parameters are computed using Eqn. (6) based on c_t, c_l, and ρ, which are considered in the theoretical calculations. Tab. 1 shows the calculated Young's modulus and Poisson's ratio for PVC and aluminum.

$$\begin{cases} c_t = \sqrt{\frac{\mu}{\rho}} \\ c_l = \sqrt{\frac{\lambda+2\mu}{\rho}} \end{cases} \tag{6}$$

Table 1. Parameters for PVC and aluminum.

	PVC	aluminum
$\lambda\ (GPa)$	3.19	59.4
$\mu\ (GPa)$	0.75	27.6
$E\ (GPa)$	2.11	74.02
ν	0.405	0.342

3.1.3 Meshing and Time Step

A Gaussian laser pulse shape with a duration of $\tau = 25\ ns$ is applied as a force. The two point thermoelastic sources are loaded with forces of $-F(t)\vec{i}$ and $+F(t)\vec{i}$ on the first and second point loads, respectively. Where $\pm\vec{i}$ represents the direction of the unit vector $\vec{i}$ along the x-axis on the substrate's surface, and the force $F(t)$ is expressed [16]:

$$F(t) = \frac{t}{\tau^2}\exp\left(\frac{-t}{\tau}\right).H(t) \tag{7}$$

Such that, $H(t)$ is the Heaviside function. The time range is set up to 10 μs for detecting dispersive signals, and a time step of $\Delta t = 4\ ns$ is chosen, satisfying Eqn. (8) [17, 18], assuming that $f_{max} = 10\ MHz$. However, the maximum element size $\Delta x = 10\ \mu m$ is applied to the three layers for a uniform mesh, based on f_{max}, which should be less than 15 μm. A coarse mesh is used in domain 4 as a PML to attenuate bulk and surface elastic waves. All these factors and dimensions are illustrated in Fig. 2.

$$\begin{cases} \Delta t < \frac{1}{20 f_{max}} \\ \Delta x < \frac{\lambda_{min}}{20} \end{cases} \tag{8}$$

3.2 Results of FEM

The Finite Element Method can help to identify the experimental solution based on physical principles. Fig. 3, shows the results at different times and the dispersion of the surface acoustic waves affected by the thickness and

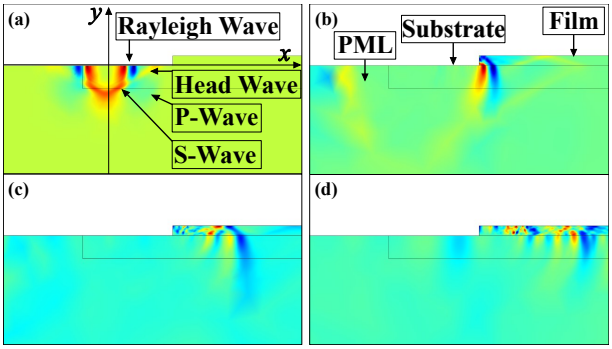

Figure 3. Surface waves at different times of flight: $t = 0.2\ \mu s$(a), $t = 0.6\ \mu s$(b), $t = 1\ \mu s$(c), $t = 2\ \mu s$(d).

Young's modulus of the intermediate layer $E_0 = 2\ GPa$ (chosen as a perfect contact condition).

At $t = 0.2\ \mu s$ (a), the effect of the force in the thermoelastic regime appears, by generating P-Wave (longitudinal wave), S-Wave (transversal wave), Head wave, and surface Rayleigh wave. At $t = 0.6\ \mu s$ (b), elastic waves are attenuated in the PML, and the Rayleigh wave interacts with the film. At $t = 1\ \mu s$ (c), the start of the guided wave reflections in the film causes dispersion. At $t = 2\ \mu s$ (d), dispersion increases as the wave propagates, and all waves are attenuated in the PML, indicating greater dispersion with a longer propagation distance.

The uniformity in the thickness and other properties of the materials in the FEM allows for flexibility in studying the impact of adhesion by altering Young's modulus of the intermediate adhesive layer, which is related to K_n and K_t (Eqn. (5)).

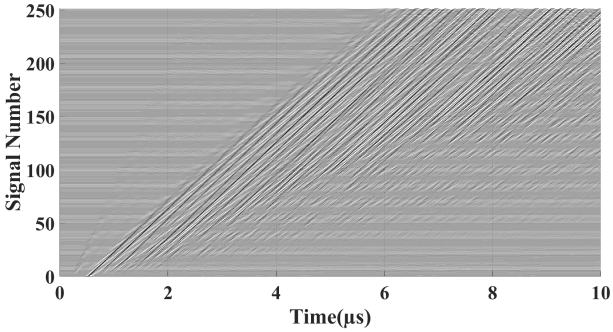

Figure 4. Signals related to the normal displacement detected at each point of the interface.

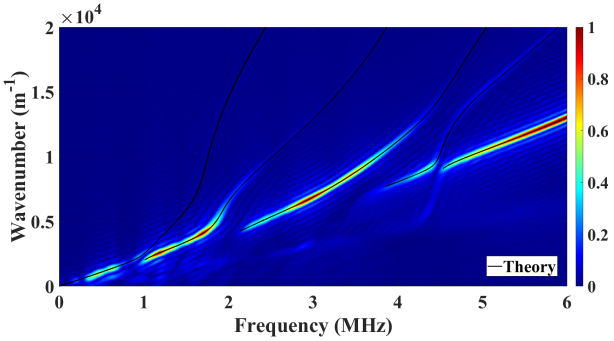

Figure 5. Wavenumber-frequency diagram obtained by FEM matching the theoretical calculation.

Fig. 4 shows the modifications of the wave amplitude and its dispersion at each detection point. Then, its corresponding wavenumber-frequency diagram by 2D Fourier transform is represented in Fig. 5 matching the theoretical calculation of the dispersion curves in the wavenumber-frequency domain. The theoretical calculation can be obtained by calculating at each frequency the values of the wavenumber for each value of the phase velocity.

These results predict that in the frequency range $f \leq 6\ MHz$, the second, third, and fifth Rayleigh modes are more likely to be detected experimentally than other modes, as it shows a maximum amplitude.

4. EXPERIMENT

4.1 Experimental Setup

In the experimental setup Fig. 6, a pulsed Nd:YAG laser is used to generate ultrasound waves in the sample. The generated surface acoustic waves propagate through the interface of the PVC film and aluminum substrate and interact with its elastic properties. The normal displacement at the surface of the aluminum substrate is detected by a laser interferometer with a filter of $4\ MHz$. Due to the fact that the PVC layer is transparent, it is then possible to generate elastic waves in the thermoelastic regime at the interface of the sample.

4.2 Nature of Adhesion

It is well known that there are many causes of the adhesion phenomenon. The PVC flexible film seems to naturally adhere to smooth aluminum surfaces when external pressure is applied. No specific deposition technique is used to

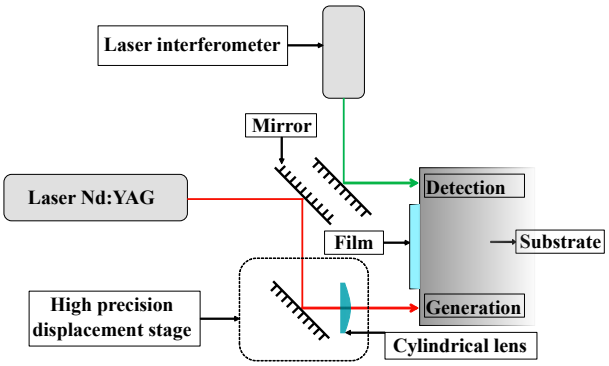

Figure 6. Experimental setup.

make the PVC film stick to the aluminum substrate, leading to the assumption that the adhesive forces are due to natural Van der Waals forces, as no other adhesive cause is applied [1]. However, two levels of adhesion were examined: the first level occurred when the film is placed on the substrate's surface directly, and the second level is achieved using a specific device.

4.3 Results and Discussion

Fig. 7 demonstrates the impact of increasing the level of adhesion on the dispersion of the Rayleigh wave. These signals correspond to the generation of Rayleigh waves at the substrate's surface, and detection at the surface after the waves pass through the sample's interface.

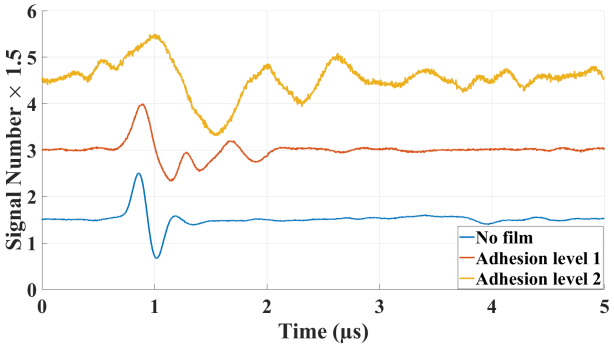

Figure 7. Effect of the adhesion level on the Rayleigh wave propagation.

At the high adhesion level (2), the film is considered in good contact with the substrate and adhesion is homogeneous along the axis of propagation at the interface, unlike the lower adhesion level (1). Therefore, 251 signals are generated along a 15 mm distance, separated by $dx = 60\ \mu m$ on the interface of the sample. These signals are processed using the 2D Fourier transform to obtain the wavenumber-frequency diagram.

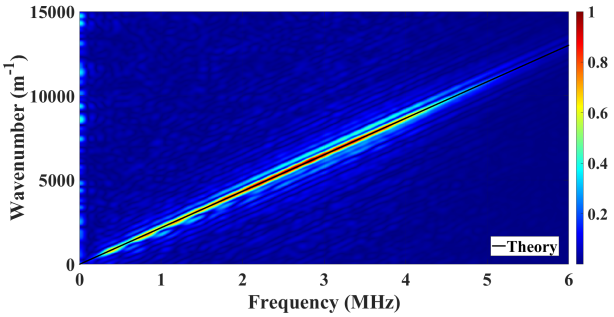

Figure 8. Wavenumber-frequency diagram of the experimental signals detected in the case of no film.

Fig. 8, shows the result of the wavenumber-frequency diagram when Rayleigh wave is generated on the aluminum substrate without the PVC layer. No dispersion is detected and the velocity remains constant ($V_p \approx 2900\ m/s$). Moreover, Fig. 9 shows the fitting of the experimental data with the theory at $K_n = 5 \times 10^{14}\ N/m^3$ and $K_t = 4 \times 10^{13}\ N/m^3$. Since no adhesive layer or specific deposition technique is used in the experiment, it can be concluded that the dispersion of the wavenumber into three distinct modes when $f \leq 3.5\ MHz$, is due to the change in adhesion level. Due to the $4\ MHz$ low-pass filter used in the detection, the amplitudes of the 4^{th} and 5^{th} modes are attenuated.

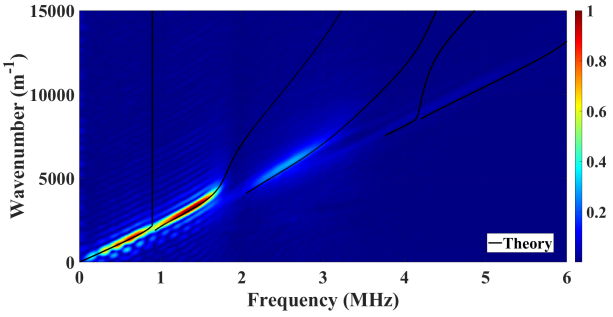

Figure 9. Wavenumber-frequency diagram of the experimental signals detected for adhesion level 2.

5. CONCLUSION

In this paper, we have examined the effect of normal and tangential stiffnesses on Rayleigh modes dispersion curves, from weak adhesion with Lamb modes in the film and no substrate influence, to strong adhesion resulting in perfect contact dispersion curves in the loading case. Additionally, the finite element method was used to study the interaction of the Rayleigh wave with the material properties as it propagates through the interface, as well as the ability to experimentally detect the modes based on the modeled maximum amplitudes.

Two adhesion levels were then studied thanks to the experimental setup. At the higher level, the film is considered in good contact with the substrate. However, the results indicated that the adhesion did not reach perfect contact condition, as far as satisfactory results correspond to values of $K_n = 5{\times}10^{14}\ N/m^3$ and $K_t = 4{\times}10^{13}\ N/m^3$.

6. REFERENCES

[1] K. Mittal, "Adhesion aspects of metallization of organic polymer surfaces," *Journal of vacuum science and technology*, vol. 13, no. 1, pp. 19–25, 1976.

[2] J. Sermeus, B. Verstraeten, R. Salenbien, P. Pobedinskas, K. Haenen, and C. Glorieux, "Determination of elastic and thermal properties of a thin nanocrystalline diamond coating using all-optical methods," *Thin Solid Films*, vol. 590, pp. 284–292, 2015.

[3] S. Fourez, F. Jenot, M. Ouaftouh, M. Duquennoy, and M. Ourak, "Non-contact thickness gauging of a thin film using surface waves and a void effect on their propagation," *Measurement Science and Technology*, vol. 23, no. 8, p. 085608, 2012.

[4] F. Faëse, F. Jenot, M. Ouaftouh, M. Duquennoy, and M. Ourak, "Laser-ultrasound-based non-destructive testing—optimization of the thermoelastic source," *Measurement Science and Technology*, vol. 26, no. 8, p. 085205, 2015.

[5] X. Xiao, Y. Sun, and X.-M. Shan, "Nondestructive determination of interfacial adhesion property of low-k/si by the surface acoustic waves," *Surface and Coatings Technology*, vol. 207, pp. 240–244, 2012.

[6] S. Mezil, F. Bruno, S. Raetz, J. Laurent, D. Royer, and C. Prada, "Investigation of interfacial stiffnesses of a tri-layer using zero-group velocity lamb modes," *The Journal of the Acoustical Society of America*, vol. 138, no. 5, pp. 3202–3209, 2015.

[7] X. Xiao, H. Qi, Y. Tao, and T. Kikkawa, "Study on the interfacial adhesion property of low-k thin film by the surface acoustic waves with cohesive zone model," *Applied Surface Science*, vol. 388, pp. 448–454, 2016.

[8] T. T. William, "Transmission of elastic waves through a stratified solid medium," *Journal of Applied Physics*, vol. 21, no. 2, pp. 89–93, 1950.

[9] N. A. Haskell, *Vincit Veritas: A Portrait of the Life and Work of Norman Abraham Haskell, 1905-1970*. American Geophysical Union, 1990.

[10] S. Rokhlin and Y. Wang, "Analysis of boundary conditions for elastic wave interaction with an interface between two solids," *The Journal of the Acoustical Society of America*, vol. 89, no. 2, pp. 503–515, 1991.

[11] G. W. Farnell and E. Adler, "Elastic wave propagation in thin layers," *Physical acoustics*, vol. 9, pp. 35–127, 2012.

[12] Y. M. Choi, D. Kang, J. N. Kim, and I. K. Park, "Evaluation of adhesion properties of thin film structure through surface acoustic wave dispersion simulation," *Materials*, vol. 15, no. 16, p. 5637, 2022.

[13] S. Sikdar and S. Banerjee, "Identification of disbond and high density core region in a honeycomb composite sandwich structure using ultrasonic guided waves," *Composite Structures*, vol. 152, pp. 568–578, 2016.

[14] J. Du, B. R. Tittmann, and H. S. Ju, "Evaluation of film adhesion to substrates by means of surface acoustic wave dispersion," *Thin Solid Films*, vol. 518, no. 20, pp. 5786–5795, 2010.

[15] M. Robin, F. Jenot, M. Ouaftouh, and M. Duquennoy, "Influence of the laser source position on the generation of rayleigh modes in a layer–substrate structure with varying degrees of adhesion," *Ultrasonics*, vol. 102, p. 106051, 2020.

[16] Y. Dai, B. Q. Xu, Y. Luo, H. Li, and G. D. Xu, "Finite element modeling of the interaction of laser-generated ultrasound with a surface-breaking notch in an elastic plate," *Optics & Laser Technology*, vol. 42, no. 4, pp. 693–697, 2010.

[17] C. Scruby and L. Drain, "Laser ultrasonics˜ adam hilger," *New York*, 1990.

[18] J. D. Achenbach, "Laser excitation of surface wave motion," *Journal of the Mechanics and Physics of Solids*, vol. 51, no. 11-12, pp. 1885–1902, 2003.